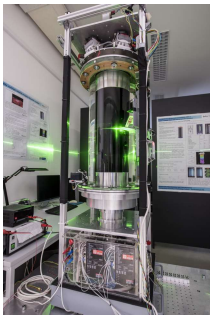


Experimental investigation of stratorotational instability using a thermally stratified system: instability, waves and associated momentum flux

Stratified vortices can be found from small to large scales in geophysical and astrophysical flows. On the one hand tornados and hurricanes can lead to devastation and even a large number of casualties, on the other hand the vortices distribute heat and momentum in the atmosphere and are hence very important for a habitable environment on Earth. In the astrophysical context, accretion disks (from which solar systems are formed) can be seen as stratified vortices. For planet formation, understanding the mechanisms that can result in an outward transport of angular momentum is a central problem. For a planet or star to be formed in a disk, angular momentum has to be carried away from its center in order to allow matter aggregation by gravity; otherwise its rotation speed would be far too large, avoiding this matter aggregation (and the consequent star formation) to happen. In such gas systems, turbulence is the most likely mechanism to achieve such a large angular momentum transport. However, it was shown that the flow profile of accretion disks is stable and the question arises how the turbulence can be generated. Among other candidates, the Strato Rotational Instability (SRI) has attracted attention in recent years. The SRI is a purely hydrodynamic instability that can be modeled by a classical Taylor-Couette (TC) system with stable density stratification due to axial salinity or temperature gradients. Much insight can be obtained from a particular designed Taylor-Couette laboratory experiment with axial stratification. In the scope of this study we investigate experimentally the phenomena associated with the instability and the nonlinear saturation of temperature stratified TC flows in a finite height cylindrical gap, and measuring the angular-momentum transport in the linear and nonlinear regimes.

Experimental setup



geometrical parameters: $r_{in} = 75 \text{ mm}$, $r_{out} = 145 \text{ mm}$, $h = 700 \text{ mm}$, $\Gamma = (r_{out} - r_{in})/h = 10$

control parameters: $\eta = r_{in}/r_{out} = 0.5172$, $\mu = \Omega_{in}/\Omega_{out}$, $N^2 = \text{sgn}(\Delta T/\Delta z)$

$Re = \frac{\Omega_{in} r_{in} (r_{out} - r_{in})}{\nu}$, $Rn = \frac{N r_{in} (r_{out} - r_{in})}{\nu}$

using different velocities of the inner and outer cylinder we obtain different rotation laws:

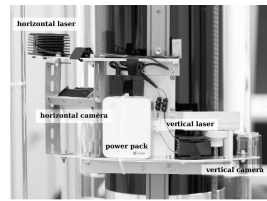
stable Taylor-Couette $\mu > \eta^2$
Keplerian $\mu = \eta^{3/2}$
Quasi-Galactic $\mu = \eta$

Working fluid: silicone oil M5 (properties at 25°C)
density $\rho = 923 \text{ kg/m}^3$
kinematic viscosity $\nu = 5 \cdot 10^{-2} \text{ m}^2/\text{s}$
coefficient of thermal expansion $\alpha(0 \dots 150^\circ\text{C}) = 1.08 \cdot 10^{-3} \text{ 1/K}$
thermal conductivity $\kappa = 0.133 \text{ W/Km}$
specific heat $c_p = 1630 \text{ J/kgK}$
Prandtl number $Pr = 56.56$

upper/lower lid heated/cooled

Measurement technique - Particle Image Velocimetry (PIV)

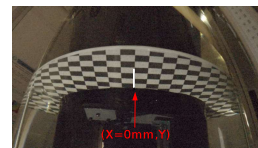
Image recording



co-rotating mini-PIV system:

'GoPro Hero 4 black edition' cameras
'medium' field of view (FOV)
resolution: 1080 x 1920 px
frame rate: 24/30 fps
recording time: = 15 min.

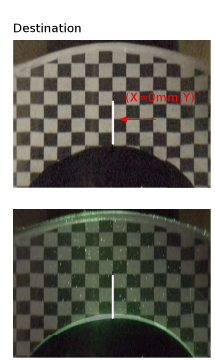
Calibration



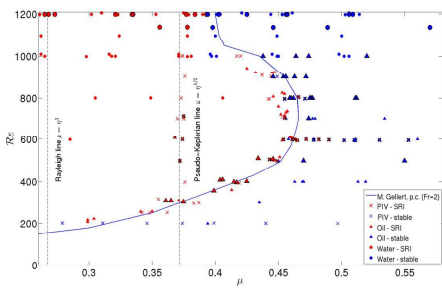
Source Image (X_s, Y_s)
Destination Image (X_D, Y_D)

$X_D = C_{21}X_s^2 + C_{20}Y_s^2 + \dots + C_{32}X_sY_s + C_{22}X_s + C_{12}Y_s + C_{00}$
 $Y_D = C_{21}X_s^2 + C_{20}Y_s^2 + \dots + C_{32}X_sY_s + C_{22}X_s + C_{12}Y_s + C_{01}$

Unix: ImageMagick
Tool: convert
Polynomial distortion



Results: Accuracy of mini-PIV

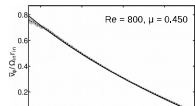
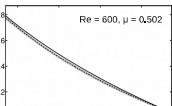


Stability diagram summarising measurements with the thermally stratified Taylor-Couette system. Red symbols show unstable flows, blue symbols stable flows. Triangles/dots indicate Kalliroscope observations using oil/water as working fluid. Crosses indicate PIV measurements. The blue solid line has been found by using the nonlinear numerical model described in Gellert and Rüdiger (2009). Note that symbols are plotted in a larger size when the condition $1.5 < Fr < Re/Rn < 2.5$ holds. Small symbols below/above $Re = 600$ usually have smaller/larger Fr.

Using $\mu = \Omega_{in}/\Omega_{out}$ and $\eta = r_{in}/r_{out}$ the analytical axially invariant solution of the angular velocity reads:

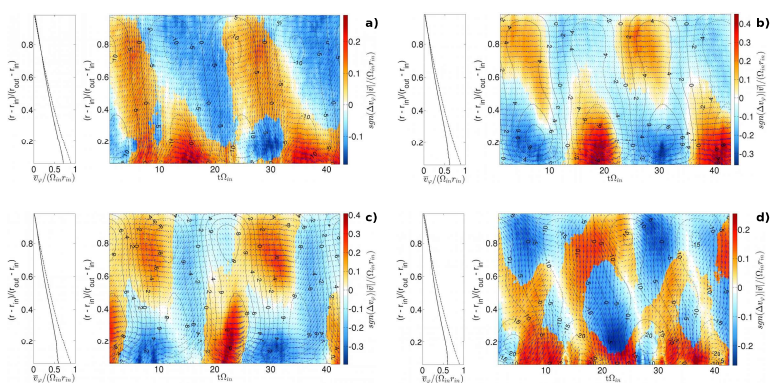
$$\Omega(r) = a + \frac{b}{r^2}, \quad a = \Omega_{in} \frac{\mu - \eta^2}{1 - \eta^2}, \quad b = \Omega_{in} r_{in}^2 \frac{1 - \mu}{1 - \eta^2}$$

Absolute error of mini-PIV: $\epsilon = 2\%$



Dashed line: Mean angular velocity in the SRI stable regime (shaded area - standard deviation).
Solid line: analytical axially invariant solution of the angular velocity

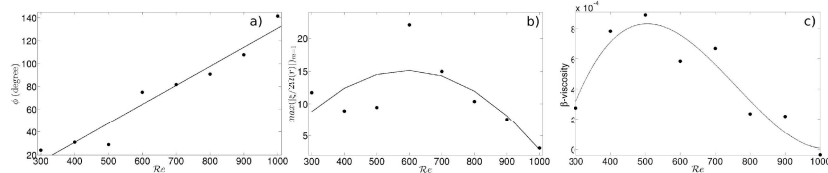
Flow structure



PIV measurements along the Keplerian line $\mu = \eta^{3/2}$ for various Re and given $Rn = 280 \pm 8.5$. Colour: Non-dimensional magnitude of the velocity perturbations $|\mathbf{v}| = (\mathbf{v}^2 + \mathbf{v}_z^2)^{1/2} / (\Omega_{in} r_{in})$, where prograde/retrograde flow is represented by red/blue, respectively. Black contour lines show the non-dimensional vertical vorticity component of the SRI mode $m = 1$ (dashed/solid - negative/positive). The non-dimensional azimuthal velocity profile averaged over time (solid line) and the non-dimensional axially invariant analytical Taylor-Couette solution (dashed line) is shown on the left side on each subfigure. (a) $Re = 300$, $Fr = 1.07$; (b) $Re = 400$, $Fr = 1.43$; (c) $Re = 500$, $Fr = 1.73$; (d) $Re = 600$, $Fr = 2.19$.

Radial flux of angular momentum along the Keplerian line $\mu = \eta^{3/2}$

Normalised Reynolds stress: $\beta_{vis} = \frac{Q_{r-\varphi}}{r_{in} \Omega_{in}^2}$, where $Q_{r-\varphi} = \langle v_r \Delta v_\varphi \rangle = \iint v_r \Delta v_\varphi dt dr$



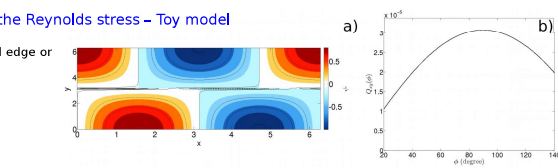
(a) Tilt ϕ of the vorticity axis of the SRI mode $m = 1$ as a function of Re (black dots). The solid line is a linear fit $\phi = 1/6Re - 35.7$.
(b) Maximum magnitude of the vorticity $|\xi|/2\Omega(r)_{max}$ (black dots). The curve shows a quadratic fit $\max(|\xi|/2\Omega(r))_{max} = -7.4 \cdot 10^{-3} Re^2 + 0.09 Re - 10.8$.
(c) β -viscosity analysed from measurements (black dots). The curve is a cubic fit $\beta_{vis} = 1.26 \cdot 10^{-11} Re^3 - 2.9 \cdot 10^{-8} Re^2 + 1.9 \cdot 10^{-3} Re - 3.25 \cdot 10^{-3}$.

Effect of the boundary wave phase shift on the Reynolds stress - Toy model

Stationary wave solution that consists of two coupled edge or boundary waves expressed by the stream function

$$\psi = \left(\frac{\tan^{-1} k(y - \pi)}{\pi} + \frac{1}{2} \right) \cos\left(\frac{1}{2}y\right) \sin(\lambda(x - \phi)) + \left(\frac{1}{2} - \frac{\tan^{-1} k(y - \pi)}{\pi} \right) \cos\left(\frac{1}{2}y\right) \sin(\lambda x)$$

Analytical solution: $Q_{xy}(\phi) \sim \lambda \sin \lambda \phi$



Toy model solution for $\phi = \pi/2$, $\kappa = 1000$, $\lambda = 1$. (a) Red/blue colour represents positive/negative stream function. (b) Reynolds stress as a function of the boundary wave phase shift ϕ . There exists an optimal $\phi = \pi/2$ where Reynolds stress is maximised.

Drift rate

Drift of azimuthal SRI modes $m = 1, \dots, 6$, $Rn = [121, 408]$, as a function of the angular velocity of the inner cylinder (dots). The solid black line is a linear fit $\dot{\phi} = 0.515\Omega_{in} + 0.0316$, regression coefficient $R = 0.988$. The dashed black line is the empirical drift derived by Rüdiger et al. (2017). The relation found by Caton et al. (2000) for SRI with resting outer cylinder is plotted as solid green line. The dashed green line shows the empirical drift derived by Rüdiger et al. (2017) with $\mu = 0$ that belongs to a resting outer cylinder.

